JCTC Journal of Chemical Theory and Computation

Article

pubs.acs.org/JCTC

Complementarity of QTAIM and ELF Partitions: Deeper Understanding of the Anomeric Effect

David Ferro-Costas* and Ricardo A. Mosquera*

Departamento de Química Física, Universidade de Vigo, Facultade de Química, Lagoas-Marcosende s/n, 36310 Vigo, Galicia, Spain

Supporting Information

ABSTRACT: In this work, fragments with chemical significance are defined inside QTAIM basins through the use of the ELF partition. In an ideal situation, core and monosynaptic ELF basins for an atom A (C_A and V_A, respectively) should belong exclusively to its atomic basin (C_A, $V_A \in \Omega_A$), while disynaptic ones ought to be divided between the atoms of the corresponding bond (for an A−B bond, $V_{A-B} \in \Omega_A \cup \Omega_B$). Several examples here analyzed verify this situation (within 0.01 au). This combined partitioning is also applied to the analysis of the conformational preference in diverse anomeric compounds. Results lead to an alternative interpretation, independent of hyperconjugative effects.

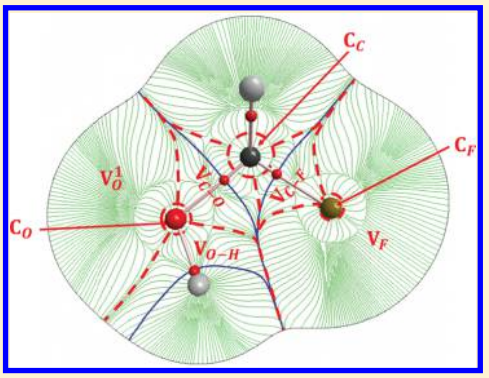

1. INTRODUCTION

Because of the bielectronic character of the electrostatic molecular Hamiltonian, most of the information stored in the wave function is irrelevant for chemical purposes. Moreover, the language of the quantum theory differs greatly from that of chemistry. For these reasons, the necessity of methods for the analysis of the electron density function (or similar ones) has acquired great importance in the field of chemistry, since (with them) a lot of concepts can be explained in words and terms normally used by chemists. QTAIM (Quantum Theory of Atoms In Molecules)[1,2] and ELF (Electron Localization Function)[3−5] analysis are two of the modern methods broadly accepted nowadays for this purpose. The first one divides the three-dimensional space, occupied by a molecule, into subelements associated with the atoms in the molecule (called atomic basins), using the electron density, $\rho(\mathbf{r})$, as the scalar function. The second one does it through the ELF, a function that can be understood as, in the words of D. B. Chesnut, "*a local measure of the Pauli repulsion between electrons due to the exclusion principle*" and that "*allows one to define regions of space that are associated with different electron pairs in a molecule.*"[6]

It is of importance to highlight that only the topological property which defines the limits of the atomic basins (the ones from QTAIM) is also of physical significance, as its definition can be obtained from quantum mechanics.[7] The integration of $\rho(\mathbf{r})$ in the atomic basins provides total atomic populations, whose variation is, unfortunately, not always easily related to chemical changes. However, despite the absence of rigorous deduction from quantum mechanical principles, ELF basins suit this task perfectly. Thus, we are in front of two different sets of basins, each one with its pros and cons. We think both partitions can be complementary and QTAIM basins can be split with ELF into fragments with clear chemical significance.

In this work, we analyze the superposition of both partitions, as well as the possibility of obtaining chemical information from it. Within our results, we find very interesting the fact that the ELF monosynaptic basins (lone pairs, lp's) are basically defined inside a single atomic basin (totally desirable when trying to understand the chemistry of every atom in the molecule) and that the merge of both QTAIM and ELF analysis mainly results in the division of the disynaptic basins into two sub-basins (each one belonging to one atom of the bond). Furthermore, the possibilities of this superposition of basins are explored, applying it to the explanation of the anomeric and *Z* effects.

Both effects refer to the preference for a specific arrangement of X−C−Y−R moieties, X being an electronegative atom and Y an atom with at least one lp of electrons.[8−11] When the central C displays a sp^3 like hybridization, the effect is called the "anomeric effect," while it is named the "Z effect" when an sp^2 like hybridization center is involved (Figure 1).

Several explanations were proposed along the years for both conformational preferences. The most common one used in chemical books is based on the hyperconjugative model[8,12] (HM). According to it, the preferred nuclear arrangements are characterized by the best hypothetical delocalization of the lp of Y over the σ^* molecular orbital (MO) of the C−X (or C═X) bond. This could explain why the gauche conformation is preferred in standard anomeric molecules, while a predilection for the Z disposition is found in anomeric systems with an sp^2 like central C (Figure 1). Nevertheless, through the use of valence bond[13−15] calculations, Mo[16] has provided strong evidence that the hyperconjugative interaction is not the

Received: July 19, 2013
Published: September 27, 2013

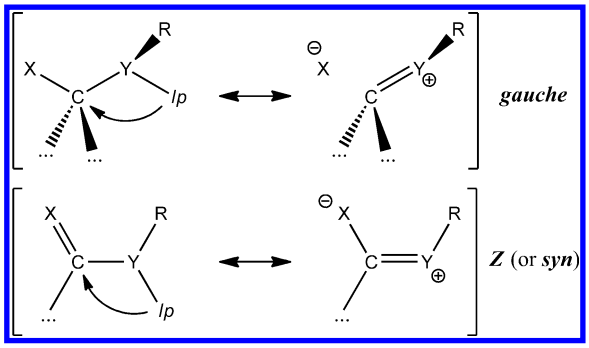

Figure 1. Preferred conformation of the X−C−Y−R moiety for anomeric (gauche arrangement) and Z (syn or Z arrangement) effects. Both resonance forms associated with the $lp_Y \rightarrow \sigma^*_{C-X}$ hyperconjugative interaction are also shown.

cornerstone of the anomeric preference, being better interpreted in terms of electrostatic interactions.

From our point of view, although we agree that the hyperconjugative model can be a useful tool for chemists, quantum mechanics provide us with more powerful theories with stronger mathematical backgrounds and physical foundations than those in which the HM rests. For this reason, we analyzed in other works the anomeric effect, using the QTAIM and an energetic decomposition scheme similar to the IQA (Interacting Quantum Atoms)[17,18] one, which rigorously allowed us to understand chemistry in terms of atoms and interactions among them. Our target molecules were the simplest ones displaying an anomeric/Z preference: fluoromethanol,[19] methanediol,[17,20] and formic acid.[17] While some results were in line with the hyperconjugative model ideas, others were not. Thus, regarding both resonance forms arising from the hyperconjugative interaction (Figure 1), a decrease on the total electronic population of Y, with regard to the opposite arrangement (gauche vs anti, Z vs E), was expected. However, opposite behavior was found.

On the other side, integrated values of ELF basins in methoxymethanol conformers were also previously employed by Chesnut to analyze the anomeric effect.[6] Significant changes were found when comparing the total electron population of the disynaptic C−O basin $N(V_{C-O})$, and that of the monosynaptic O lp, $N(V_O)$, in the conformers with gauche and antiperiplanar arrangements for the R−O−C−X moiety. Internal rotation from anti to gauche increased $N(V_{C-O})$ and reduced $N(V_O)$. These facts seem to be in accordance with a larger participation of the double-bond/no-bond resonance structure for the $ROCH_2X$ fragment in the gauche conformer, usually invoked by hyperconjugative explanations of the anomeric effect.

We think that studying our system models again through the analysis of different fragments inside the QTAIM atoms, defined with chemical significance thanks to the ELF, can be of interest and that it will help us to get a deeper understanding of these systems. We expect that this combined partition, which should resemble the simple chemical picture of atoms, bonds, and lone pairs, could enlighten whether or not hyperconjugation is really of relevance within the anomeric effect.

2. COMPUTATIONAL DETAILS

2.1. Partition of the Space by the Gradient Field of a Scalar Function. The gradient vector field of a scalar function $\mathcal{V}(\mathbf{r})$ is represented through a display of trajectories traced out by the vector $\nabla\mathcal{V}(\mathbf{r})$. Any trajectory of $\nabla\mathcal{V}(\mathbf{r})$ from an arbitrary point originates or terminates at a critical point in $\mathcal{V}(\mathbf{r})$. The set of points whose trajectory ends in the same point A defines the basin of attraction for A. In this open set containing A, every point sufficiently close to A is attracted to A. The separatrix of the basin of attraction is a surface (S) of zero flux in the gradient vectors of the scalar function (eq 1). Thereby the three-dimensional space can be split into attraction basins through the use of a scalar function.

$$\nabla\mathcal{V}(\mathbf{r})\cdot n(\mathbf{r}) = 0 \quad \forall\ \mathbf{r} \in S \tag{1}$$

In the case of QTAIM, the scalar function used for the division is the electron density, $\mathcal{V}(\mathbf{r}) = \rho(\mathbf{r})$. As remarked in the Introduction, its topological property (eq 1) can be obtained as a mechanical definition from quantum mechanics: it rises up after the generalization of the action principle to a subsystem of some total system.[1]

2.1.1. Electron Localization Function. The spherically averaged conditional pair probability, $P^{\sigma,\sigma}(\mathbf{r},s)$, represents the probability of finding, once an electron is situated at $\mathbf{r}$, another electron of the same spin (σ) at a distance of s. The Taylor expansion of this probability, for monodeterminantal Hartree−Fock (HF) wave functions,[21] is given by eq 2, where τ_σ is the positive-definite kinetic energy density ($\sum_{i=1}^{\sigma}|\nabla\phi_i|^2$, where the summation is restricted only to molecular orbitals of σ spin) and ρ_σ is the σ-spin electron density. As "*the smaller the probability of finding a second like-spin electron near the reference point, the more highly localized is the reference electron*,"[3] the electron localization can be related to the smallness of D_σ (eq 2), which is the Laplacian of the conditional probability calculated from a single determinantal HF wave function. As a consequence of this "inverse relationship"(localizability $\leftrightarrow D_\sigma$), the electron localization function (ELF, η) is defined according to eq 3, D_σ^0 corresponding to a uniform electron gas with spin-density equal to the local value.

$$P^{\sigma,\sigma}(\mathbf{r}, s) = \frac{1}{3}D_\sigma(\mathbf{r})s^2 + \ldots = \frac{1}{3}\left[\tau_\sigma(\mathbf{r}) - \frac{1}{4}\frac{|\nabla\rho_\sigma(\mathbf{r})|^2}{\rho_\sigma(\mathbf{r})}\right]s^2 + \ldots \tag{2}$$

$$\eta(\mathbf{r}) = \left[1 + \left(\frac{D_\sigma(\mathbf{r})}{D_\sigma^0(\mathbf{r})}\right)^2\right]^{-1} \tag{3}$$

When $\eta(\mathbf{r})$ becomes the scalar function $\mathcal{V}(\mathbf{r})$ in eq 1, basins within which one or more electron pairs are to be found can be defined.[6] Two different kinds of ELF basins can be obtained: those containing a nucleus (different from H), called *core basins* (C_X; X being a nucleus), and those without it (or with a H nucleus), *valence basins*. The latter are defined by their synaptic order: monosynaptic when connected only to one core basin (e.g., lone pair of atom X, V_X), disynaptic when connected to two core basins (e.g., covalent bond between A and B atoms, V_{A-B}), etc. Hydrogen basins are considered valence ones (and not core) as they represent a shared pair of electrons (V_{A-H} for the A−H bond).

2.2. ELF∩QTAIM Partitioning Scheme. The superposition of ELF basins upon the QTAIM partition allows us to understand a Ω atomic basin as a set of sub-basins with chemical significance. Thereby the electron population of an atomic basin (eq 4) can be split into different terms, according

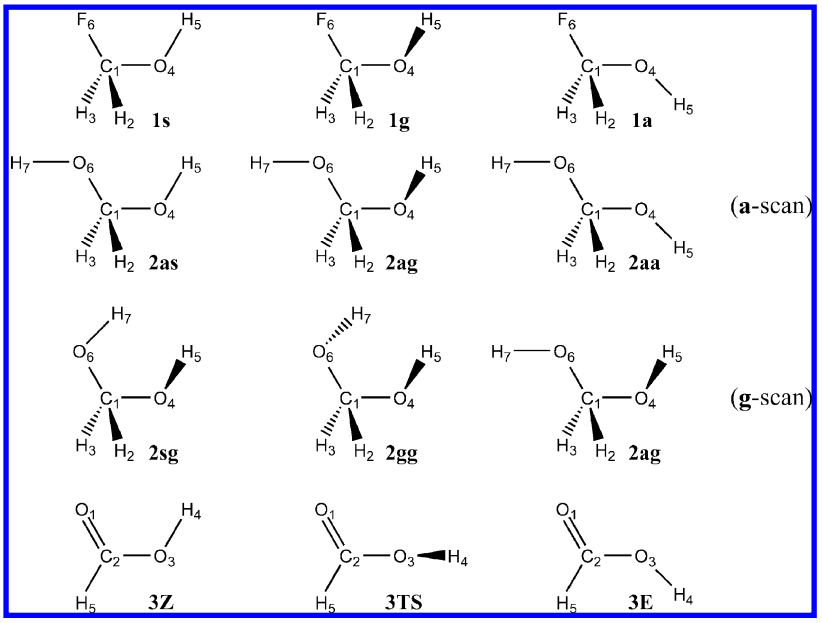

Figure 2. Characteristic nuclear arrangements in the energy scans performed for all the systems. Nomenclature and atom labels are also shown.

to eq 5,[22] where M is the number of nuclei, $N(B \cap \Omega)$ represents the contribution of the ELF basin B to the population of the atomic basin Ω, C_i is the core basin of atom i, V_i^k is the kth ELF monosynaptic basin of atom i, and V_{i-j}^k is the kth ELF disynaptic basin of the $i-j$ bond.

$$N(\Omega) = \int_\Omega \rho(\mathbf{r})\, d\mathbf{r} \tag{4}$$

$$N(\Omega) = \sum_i^M N(C_i \cap \Omega) + \sum_i^M \sum_k N(V_i^k \cap \Omega) + \frac{1}{2}\sum_i \sum_{j\neq i} \sum_k N(V_{i-j}^k \cap \Omega) \tag{5}$$

In the ideal situation, according to the traditional chemical picture of a molecule, each QTAIM atomic basin would be composed of the corresponding set of core and monosynaptic basins (ω represents the nucleus associated with the Ω basin) and of the contribution of all the disynaptic basins ω involved (eq 6).

$$N(\Omega) = N(C_\omega) + \sum_k N(V_\omega^k) + \sum_{j\neq\omega} \sum_k N(V_{\omega-j}^k \cap \Omega) \tag{6}$$

If this happens, the ELF∩QTAIM scheme narrows down to the distribution of ELF disynaptic basins between the corresponding two atomic basins.

2.3. Generation and Integration of ELF∩QTAIM Basins. Atomic (QTAIM) and ELF basins were generated using the near-grid method with a boundary refinement step,[23] employed in Multiwfn[24] as the default method, and stored in ".cub" files. The grid is the same for each basin, but a value of 1 or 0 is associated with every point, depending on whether or not it belongs to the corresponding basin. Once all these 0/1 vectors for each basin are read, the product of the value for the Ω basin by the one for the B_i ELF basin at a point indicates if it belongs or not to the sub-basin $B_i \cap \Omega$. Doing this for all the points entails the definition of a new 0/1 vector, which describes $B_i \cap \Omega$. Obviously, the union of all these sub-basins for a corresponding atomic basin redefines it again. This is $(B_1 \cap \Omega) \cup (B_2 \cap \Omega) \cup ... \cup (B_{nelf} \cap \Omega) = \Omega$, nelf being the number of ELF basins.

The integration of $\rho(\mathbf{r})$ in the sub-basins was carried out with a multilevel refinement. When the value of the electron density (in au) at a point is in the range (0.1,0.5], (0.5,1.0], or (1.0,∞), its value is averaged calculating it in 8, 125, or 343 points homogeneously distributed in the volume associated with the original point. In other words, this volume is transformed (during basin integration) to 2^3, 5^3, and 7^3 parallelepipeds, while the one having a function value less than 0.1 au remains unchanged. In this manner, the integration accuracy of $\rho(\mathbf{r})$ will be significantly improved in the regions close to nuclei.

For a given sub-basin, its electron population is obtained by elementary numerical integration, as shown in eq 7, where npts is the number of points defining the grid, Vol_j is the volume associated with the jth point of the grid, $\overline{\rho}(\mathbf{r}_j)$ is the averaged value of the electron density at $\mathbf{r}_j$, and $(0/1)_j^{i,\Omega}$ is the 0/1 vector which defined whether the jth point belongs or not to the $B_i \cap \Omega$ sub-basin.

$$N(B_i \cap \Omega) \approx \sum_{j=1}^{npts} (0/1)_j^{i,\Omega} \cdot \overline{\rho}(\mathbf{r}_j) \cdot \mathrm{Vol}_j \tag{7}$$

2.4. Anomeric Systems: Level of Calculation and Nomenclature. Three molecules were studied: fluoromethanol (**1**), methanediol (**2**), and formic acid (**3**). For all of them, relaxed and rigid scans have been performed, varying the X−C−O−H dihedral angle (hereafter denoted as φ_i for molecule i) from 180° (**a**, anti conformation) to 0° (**s**, syn conformation) in steps of 10°. As two O−C−O−H dihedral angles can be defined in **2**, two different scans have been done. In the first scan (a-scan), one dihedral angle ($\varphi_{2,1}$ = O4−C1−O6−H7, Figure 2) is fixed at anti disposition (180°), while the other ($\varphi_{2,2}$ = O6−C1−O4−H5) is swept. During the second one (g-scan), $\varphi_{2,2}$ is fixed at 60° (point of less energy in the previous scan), while $\varphi_{2,1}$ is scanned.[25]

For X−C−O−H rigid rotations, the reference geometry corresponds to that of 180° at the relaxed scan. The most significant nuclear arrangements of these molecules along

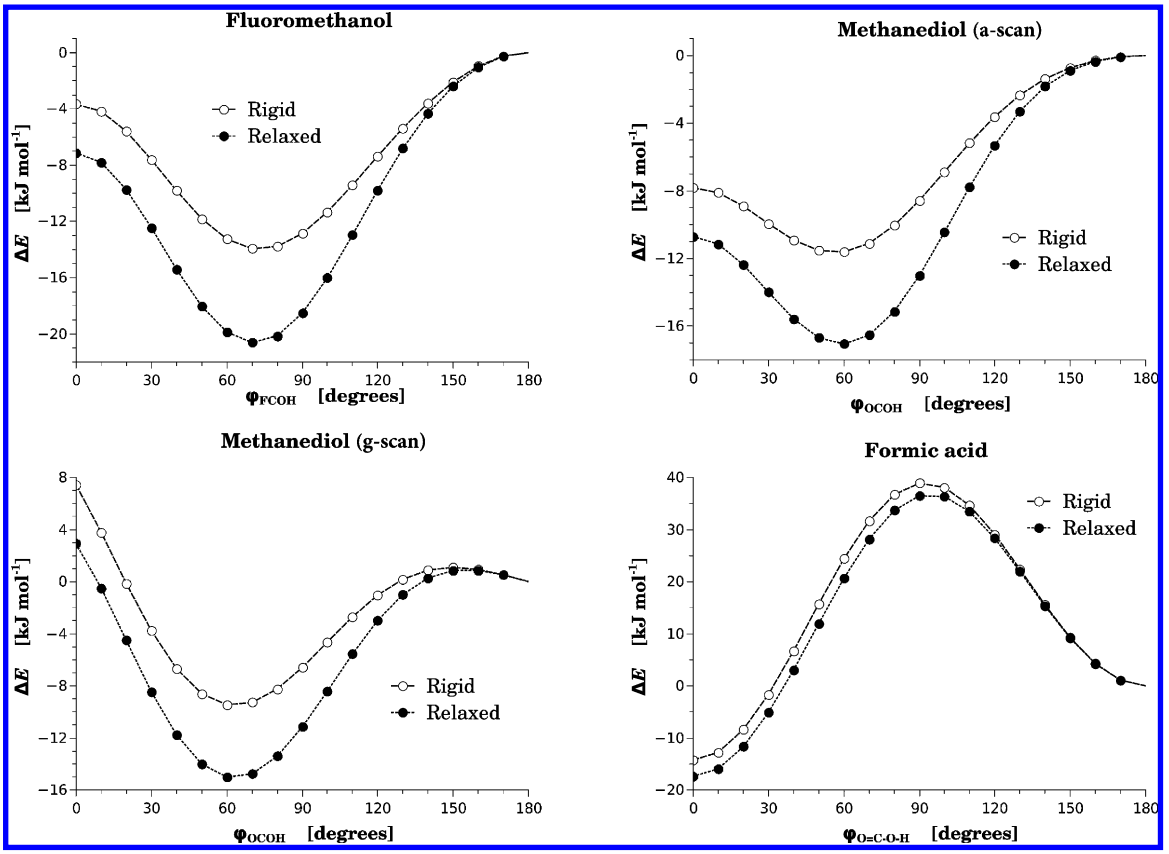

Figure 3. B3LYP/6-311++(2d,2p) 6d potential energy curves for the rotation of the X−C−O−H dihedral angle in **1** (X = F), **2** (X = OH), and **3** (X = O, sp^2 like hybridization at C).

Table 1. ELF Contributions to the Electron Population of Every QTAIM Basin for the 1s Optimized Geometry (restricted to φ_1 = 0°) of Fluoromethanol[a]

$B_i \backslash \Omega_j$	C1	H2	H3	O4	H5	F6	$\sum_j B_i \cap \Omega_j$
C_{C1}	**2.093**	0.000	0.000	0.000	0.000	0.000	2.093
C_{O4}	0.000	0.000	0.000	**2.124**	0.000	0.000	2.124
C_{F6}	0.000	0.000	0.000	0.000	0.000	**2.138**	2.138
V_{O4}	0.002	0.000	0.000	**4.735**	0.000	0.000	4.737
V_{F6}	0.001	0.000	0.000	0.000	0.000	**6.797**	6.798
V_{C1-H2}	**1.138**	**0.962**	0.000	0.004	0.000	0.011	2.115
V_{C1-H3}	**1.138**	0.000	**0.962**	0.004	0.000	0.011	2.114
V_{C1-O4}	**0.385**	0.000	0.000	**0.993**	0.000	0.000	1.378
V_{C1-F6}	**0.184**	0.000	0.000	0.000	0.000	**0.678**	0.863
V_{O4-H5}	0.000	0.000	0.000	**1.226**	**0.411**	0.001	1.637
$\sum_i B_i \cap \Omega_j$	4.940	0.962	0.962	9.085	0.411	9.636	25.997

[a]Columns represent atomic basins (Ω_j), whereas rows represent ELF ones (B_i). Monosynaptic ELF basins for an atom A are merged in a single superbasin $V_A = \sum_k V_A^k$. The sums recover the population of every basin (as well as the molecular electron population). All values are in au.

energy scans are represented in Figure 2, where nomenclature and atom labels are also shown.

All calculations were performed using the Gaussian 09[26] program with the standard 6-311++(2d,2p) 6d basis set at the B3LYP level.

3. RESULTS AND DISCUSSION

3.1. Energy Scan for X−C−O−H Molecules. For anomeric molecules **1** and **2**, one minimum (corresponding to gauche conformation, **g**) is found in each 1D scan (Figure 3). When C presents sp^2 like hybridization (formic acid, **3**), two minima appear (Z and E arrangements), whereas the saddle point between them (**3TS**) corresponds to an approximately perpendicular dihedral angle.

3.2. Full ELF∩QTAIM Scheme for Some Geometries. We have analyzed the ELF contributions to the QTAIM basins for the next optimized nuclear arrangements of the three molecules:

- **1s** (φ_1 = 0°), **1g** (φ_1 = 71.1°), and **1a** (φ_1 = 180°) for fluoromethanol
- **2ss** ($\varphi_{2,1},\varphi_{2,2}$ = 0°), **2gg** ($\varphi_{2,1},\varphi_{2,2}$ = 62.5°), and **2aa** ($\varphi_{2,1},\varphi_{2,2}$ = 180°) for methanediol
- **3Z** (φ_3 = 0°), **3TS** (φ_3 = 94.5°), and **3E** (φ_3 = 180°) for formic acid

dx.doi.org/10.1021/ct400630f | J. Chem. Theory Comput. 2013, 9, 4816−4824

In all the cases (Table 1 and Supporting Information), the ideal situation described by eq 6 is basically achieved. For example, in the case of syn fluoromethanol (**1s**, $\varphi_1 = 0°$, Table 1), we observe how each core ELF basin contributes exclusively to the corresponding atomic basin. Lone pairs also show ideal behavior, as they are mainly confined in their corresponding QTAIM basin. This ideal trend is nearly found for disynaptic basins: they basically contribute to the atoms involved in the corresponding bond. Only C−H disynaptic basins have a non-negligible (but still of minor importance) contribution in the F atomic basin (0.011 au). This ideal behavior is also clearly observable in Figure 4, where both (QTAIM and ELF) partitions are superposed.

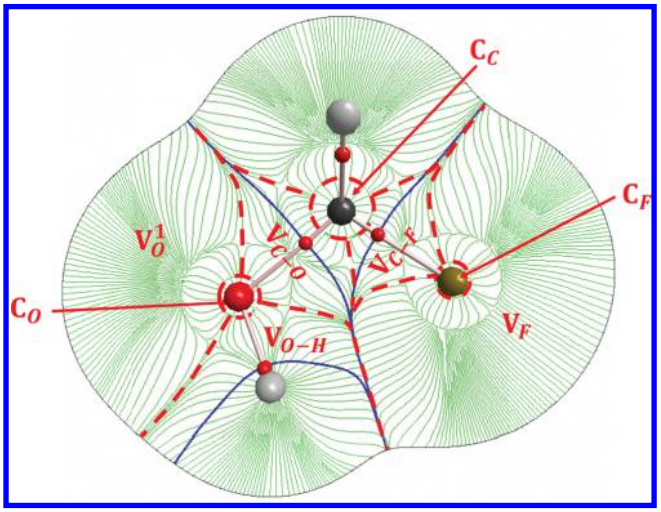

Figure 4. Gradient lines (green) of ELF at **1s** geometry, limited by a 0.001 au electron density isocontour, in the symmetry plane. Limits of the ELF basin are drawn with red dashed lines. QTAIM basin separatrices are also shown with blue continuous lines. Small red circles, which lie on the QTAIM separatrices, represent the position of bond critical points.

Thus, as eq 6 is basically correct for all the systems here studied (Table 1 and Supporting Information), we are going to consider it from now on, instead of the full partition provided by eq 5.

3.3. Anomeric Effect in Fluoromethanol. *3.3.1. Rigid Rotation.* As previously noted,[27] the role of geometry relaxation has to be decoupled from that of rigid rotation to analyze the effects of hyperconjugative interactions. Because of that, we are going to consider this kind of rotation here, dealing in the next section with the subsequent geometry relaxation. The way the electron population, N, of the ELF fragments for each QTAIM basin evolves along the rigid rotation is shown in Figures 5 and 6. As expected, all core basin populations remain basically constant along the whole rotation (Figure 5b−d). The most important variation along the rotation consists of the redistribution of $\rho(\mathbf{r})$ within the oxygen environment, mainly ascribed to the interchange of electron population between its lone pairs (as shown in Figure 6, which depicts the evolution of oxygen ELF monosynaptic basins).

This reorganization reaches its maximum value around 130°, where the oxygen lp eclipsing F(V_O^2) sends part of its electron density basically to the other lone pair (V_O^1), synperiplanar to one methylene hydrogen (Figure 7).

Looking at the evolution of N for ELF basins from 180° to 60° (Figure 5), we find that the total population of the oxygen electron lone pairs and $N(V_{F-C})$ decreases, while $N(V_{C-O})$ increases. This fact seems to be in line with the hyperconjugative interpretation of anomeric effect, as Chesnut also pointed out in previous work.[6] It is important to note that the minimum N for oxygen lp's appears at 80° and not at the **1g** conformer.

Nevertheless, we think that an alternative interpretation, more complete and where hyperconjugative interactions are not invoked, can be obtained from data. For this purpose, let us first analyze atomic populations one by one, paying attention to their ELF fragments, in order to get better insight:

•**H3** (Figure 5a): The variation of N(H3) is close to the expected trend, in accordance with the evolution of the repulsion by oxygen lp's (Figure 7). Thus, the variation of this repulsion and that of N(H3) display an inverse relationship. Accordingly, N(H3) decreases from 180° to 60° and recovers (progressively from 60° to 0°) the value exhibited at $\varphi_1 \approx 120°$.

•**H2** (Figure 5a): As H3, its variation also seems to be guided by the intensity of its repulsion by O-lp's, which is mainly increased from 60° to 0° (Figure 7).

•**H5** (Figure 5a): Its population remains almost constant from 180° to 60°, decreasing when it approaches close enough to F (from 60° to 0°, Figure 7).

•**O** (Figure 5b): Its total population basically varies according to the variation suffered by H5 along the rigid rotation, receiving the ρ donated by H5 or vice versa (Figure 8a). In other words, in this kind of rotation, the O−H fragment has the earmarks of an isolated moiety in the molecule. At the same time, the electron density of the oxygen basin reorganizes along the rigid rotation, modifying how it is distributed into mono- and disynaptic ELF regions. Thus, we observe (i) an interchange of N between lone pairs (Figure 6) and (ii) a donation from lone pairs to disynaptic fragments, $V_{C-O} \cap \Omega_O$ and $V_{O-H} \cap \Omega_O$ (Figure 8a).

•**C** (Figure 5c): As C is the basin showing more connections/bonds and it is situated at the center of the system, its behavior depends strongly on its surroundings. However, O−H chiefly behaves as an independent fragment along rigid rotation, simplifying the problem. We observe that N(C) varies according to how N(H3) does (Figure 8b). Nevertheless, the magnitude of its variation is smaller, which indicates depletion of electron density in certain regions of the carbon atom, probably in order to avoid a huge increase in the electron−electron repulsion within the atomic basin. This depletion is very notorious at the C−F fragment (Figure 5c), where part of its ρ is transferred to the closest and strongest attractor, F.

•**F** (Figure 5d): As expected, the variation in N(F) depends, basically, on the variation of $N(V_{C-F} \cap \Omega_C)$. Thus, the electron density lost by the whole ELF V_{C-F} basin is basically sent to the F lone pair regions (Figure 8c).

Although this analysis has led to an improvement in the understanding of how $\rho(\mathbf{r})$ is reorganized within and between QTAIM basins, there are some points, related to O lp's, that need to be deeply clarified. Of both O lone pairs, the one whose ΔN profile should be easily predictable is V_O^2, as it is the one which suffers directly the strong interaction with F. Moreover, as lone pairs neither have a ρ-attractor inside nor are placed between nuclei, their electron population should be the most easily modifiable (a fact confirmed by Figure 6). As a consequence, lp's are expected to interchange electron density easily between them. Obviously, during this process, other regions of the oxygen can be also modified, and part of the ρ

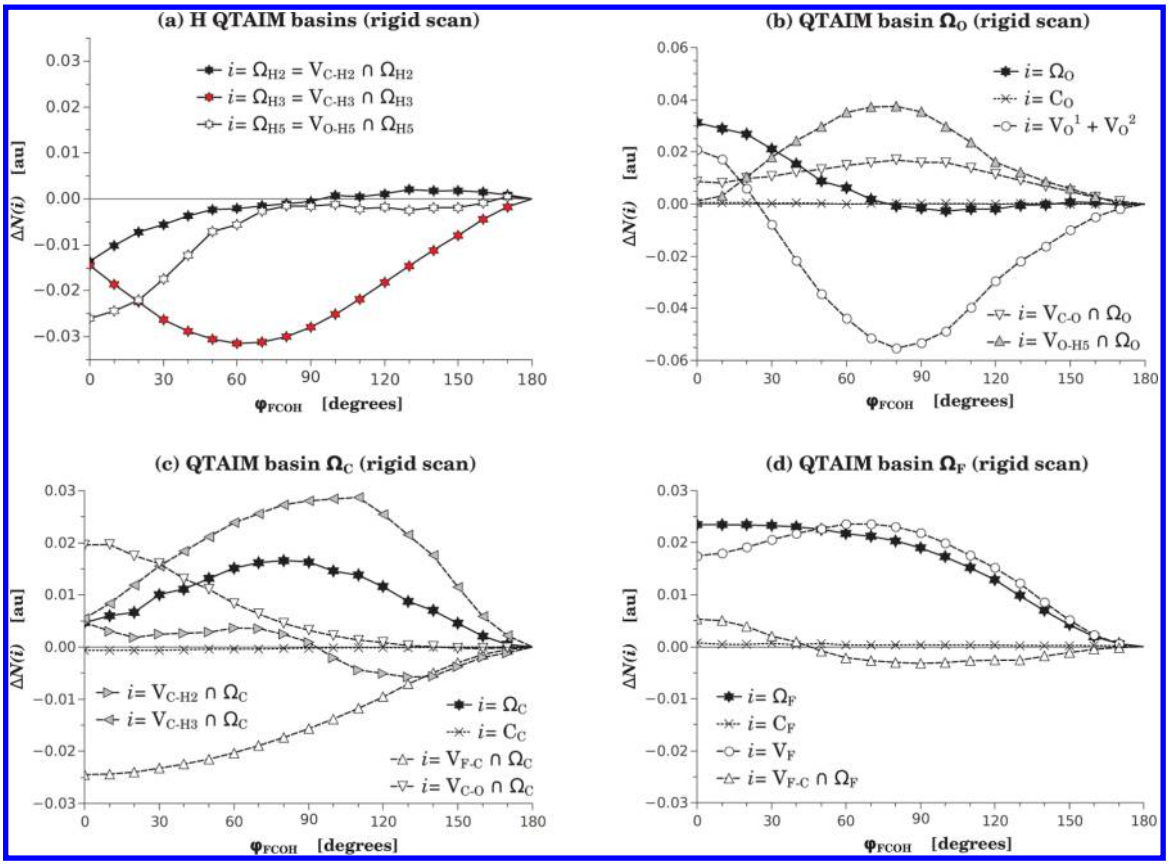

Figure 5. Evolution of QTAIM atomic populations along the C−O rigid rotation (six-point stars, linked by continuous segments) for fluoromethanol. The evolution of the ELF-fragments for each QTAIM basin is also shown (× for core basins, circles for monosynaptic basins, and triangles for disynaptic ones).

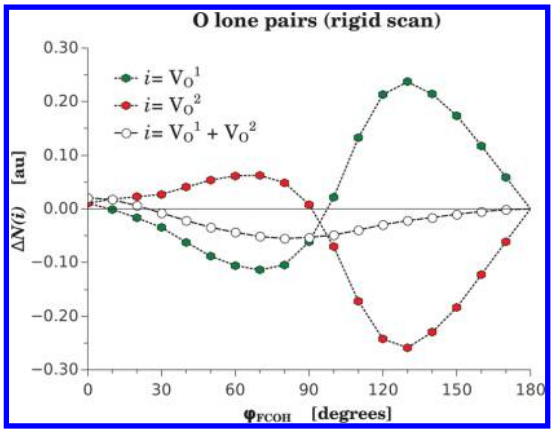

Figure 6. Evolution of both oxygen lone pair populations along rigid rotation for fluoromethanol. V_O^1 refers to the one whose ELF-attractor is situated in anti (with regard to F) at $\varphi_1 \approx 60°$, whereas V_O^2 to the one eclipsing F at $\varphi_1 \approx 120°$.

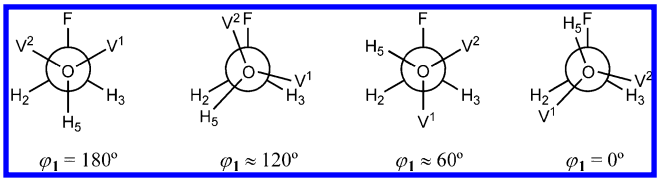

Figure 7. Fischer projections of the most significant nuclear arrangements emerging from the rigid rotation of fluoromethanol. Lone pairs of oxygen are represented as V^1 and V^2.

transferred between lone pairs may be retained in C−O and O−H ELF fragments of the O atom. The latter explains the net loss of ρ by the O lone pairs.

Regarding the $N(V_O^2)$ profile, as it gets closer to F (180° to 120°, Figure 7), it loses ρ (which is sent to V_O^1). From 120° to 60°, the situation is reversed, and it moves away from F, with the resulting increase of electron population. Finally, from ∼60° to 0°, a loss of electron density is observed as it gets eclipsed by H3.

3.3.2. Geometry Relaxation. Let us point to the rigid φ_1 = 70° arrangement as our target conformation, as it will end up in the closest geometry to the gauche conformer in the relaxed scan for this system. As described in the previous section (and schematized in Figure 9a), bond fragments associated with C−O undergo an increase of N, whereas a decrease is observed in C−F ones. These variations are in accordance with the subsequent evolution of their bond distance from rigid to relaxed structure: shrinking of C−O (−0.020 Å) and elongation of C−F (+0.027 Å), standard fingerprints of the anomeric effect.

ELF∩QTAIM analysis allows one to describe electron density reorganizations accompanying bond lengthening and shrinking. In the geometry relaxation, as the C−O bond shortens, part of its electron density is accumulated at the region belonging to the most electronegative atom. This is $\Delta N(V_{C-O} \cap \Omega_O) > 0$ and $\Delta N(V_{C-O} \cap \Omega_C) < 0$ (Figure 9b). Moreover, the population of the former region is also increased by a ρ-transfer from O lone pairs. The opposite trend is found in the enlargement of the C−F bond (Figure 9b). Its ρ

dx.doi.org/10.1021/ct400630f | J. Chem. Theory Comput. 2013, 9, 4816−4824

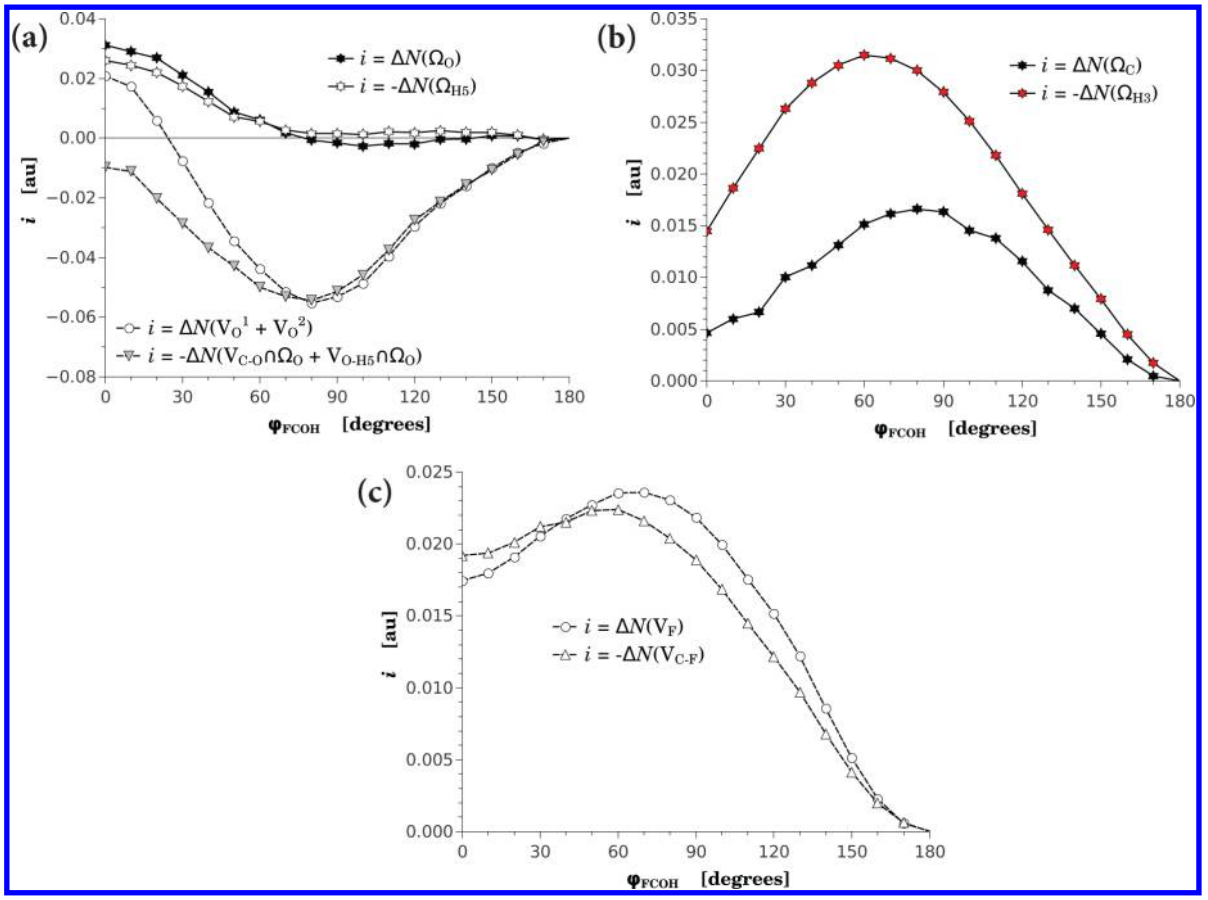

Figure 8. Diverse useful comparison of electron population profiles for the rigid rotation of fluoromethanol, used to get insight about electron density reorganization (see text).

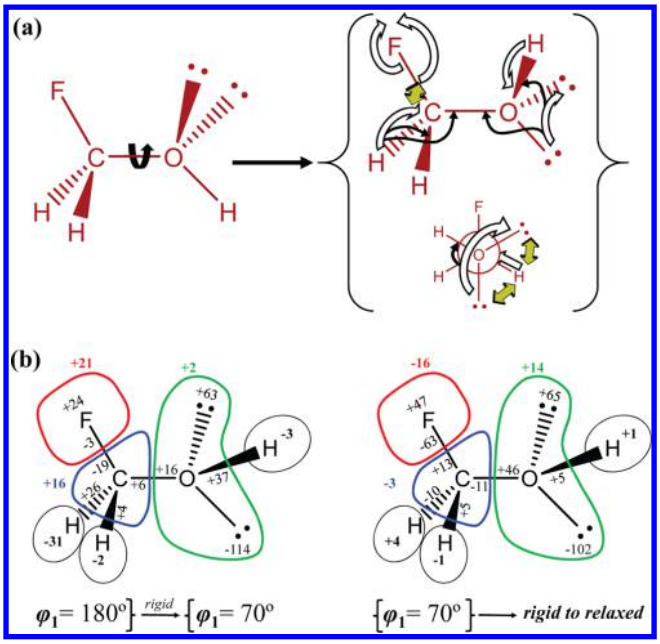

Figure 9. (a) Scheme of ρ reorganization (white and black arrows) that takes place in the evolution from **1a** to **1g** (yellow double arrows indicate repulsions which distort the electron density distribution) and (b) ΔN values (in au and multiplied by 10^3) for all the QTAIM and valence ELF∩QTAIM basins in the rigid rotation to $\varphi_1 = 70°$ and in the subsequent nuclear relaxation.

reorganization points in the same direction as the homolytic cleavage (populations of core and monosynaptic ELF basins do not exceed 9.0 au), withdrawing shared electron density from fluorine to C and to F lone pairs. Thus, ρ redistribution within a C−Z bond (Z being an electronegative atom) behaves consistently based on whether the bond is stretched or shortened (Figure 10).

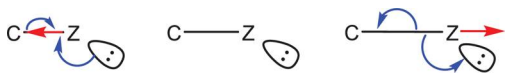

Figure 10. Scheme of the behavior of a C−Z bond when elongated and shrunk.

As in the rigid rotation, the V_O^1 lone pair suffers a depletion of electron density in its ELF basin which is reorganized within the O atomic basin (Figure 9b).

3.4. Anomeric Effect in Methanediol: a-scan. The rigid interconversion from **2aa** to **2ag** exhibits the same patterns observed in the case of fluoromethanol (Figures 9b and 11a.1). The claim made in the previous section about the reorganization inside the C basin may be ascribed to the relative disposition of the O−H fragment seems to be confirmed, as C behaves similarly in this case. However, as X has changed (from F to a hydroxyl group), the magnitude of the reorganization within O4 is now smaller. Moreover, the reorganization within the X group is different from F. In this case, the population of the $V_{C-X} \cap \Omega_X$ fragment increases continuously along the rigid rotation while depletion and

dx.doi.org/10.1021/ct400630f | J. Chem. Theory Comput. 2013, 9, 4816−4824

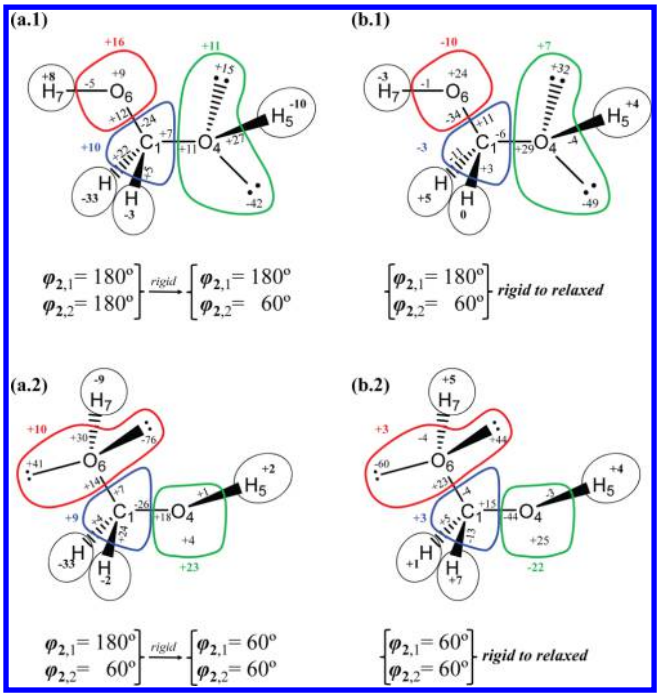

Figure 11. Same as Figure 9b, for **a**- (a.1 and b.1) and **g**- (a.2 and b.2) scans of methanediol.

increased intervals can be observed when X = F (Figure 5 and Supporting Information). Nevertheless, $\Delta N(X)$ profiles for X = F and X = OH show similar behavior (Supporting Information, Figure S12).

Leading trends observed in geometry relaxation of fluoromethanol also apply to this case ($\varphi_{2,1}$ = 180° and $\varphi_{2,2}$ = 60°, Figure 11b.1). Once again C−Z bonds behave according to Figure 10 (C1−O4 bond distance shrinks 0.014 Å, C1−O6 lengthens 0.017 Å).

3.5. Anomeric Effect in Methanediol: g-scan. The reference geometry for both g-scans (rigid and relaxed) is the one of minimum energy obtained in the relaxed a-scan of methanediol ($\varphi_{2,1}$ = 180° and $\varphi_{2,2}$ = 60°). Now, the local symmetry exhibited by the X-CH_2 moiety in previous cases (fluoromethanol and a-scan of methanediol) is broken (X being O4−H5 group in this situation). Because of this change, the reorganization inside the O6−H7 system is different from that of O4−H5 along the a-scan. This difference sharpens in the fragments that are more susceptible to change: the lone pair in gauche to X sends electron density to the other one (antiperiplanar to X). The rest of the system basically behaves as observed in the previous rotation (Figure 11).

3.6. Z effect in Formic Acid. Previously, QTAIM analysis of Z and E conformers of formic acid revealed the leading role of the O1···H4 interaction in the preference for the Z conformer.[17] It was also shown that the electron population of each atom of the O=C−O moiety was enlarged in Z at the expense of both hydrogens.

The use of the ELF∩QTAIM population scheme, which allows a deeper analysis of the Z/E equilibrium, indicates that:

•In Z and E conformations (both obtained from rigid and relaxed scans), O3 lone pairs are found described by a single monosynaptic basin whose electron population barely varies from one arrangement to the other (Figure 12). Its small reduction, slightly bigger between relaxed conformations (−0.008 vs −0.014 au), is apparently transferred to $V_{C-O3} \cap \Omega_{O3}$ and $V_{O3-H4} \cap \Omega_{O3}$.

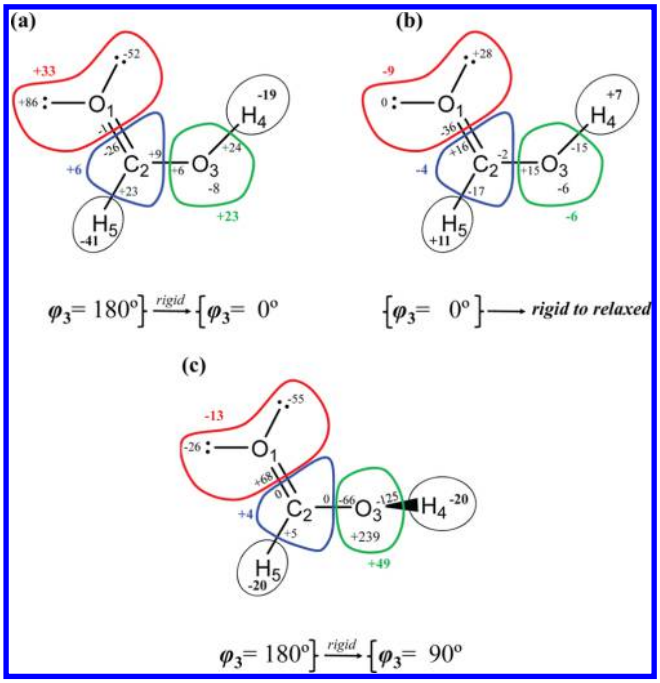

Figure 12. ΔN values (in au and multiplied by 10^3), of all the QTAIM and valence ELF∩QTAIM basins, for (a) the rigid rotation to φ_3 = 0° (E to Z), (b) the subsequent nuclear relaxation at that conformation, and (c) the rigid rotation of φ_3 from 180° to 90°.

•While the N(H4) depletion seems to transfer electron density to $V_{O3-H4} \cap \Omega_{O3}$, the electron density displaced from H5 forces a redistribution of $\rho(\mathbf{r})$ even beyond C, reaching mainly O1.

•Electron density redistribution in O1−C, C−O3, and O−H bonds during relaxation (at Z geometry, Figure 12b) presents the trends previously commented upon for both the shrinking and elongation of C−Z bonds (Figure 10).

As it is well-known, the π resonance delocalization in the O=C−O moiety breaks at φ_3= 90° (**3**⊥). This is reflected in the ELF∩QTAIM analysis as two atomic electron density reorganizations, affecting O1 and O3 (Figure 12c). The electron density of the O1−C2 bond is reinforced in the O1 region, in contrast to the loss suffered by the C−O bonding region of O3. Moreover, both $\Delta N(V_{O1-C2} \cap \Omega_{O1})$ and $-\Delta N(V_{C2-O3} \cap \Omega_{O3})$ profiles are essentially identical along the rigid rotation (Supporting information, Figure S17), which clearly indicates that there is an electron density transference between these regions (reaching a value of 0.07 au at **3**⊥ with regard to **3E**). This result is in accordance with the breaking and formation of π resonance in the O=C−O moiety, which takes place along the rigid rotation. We realized that this trend is hidden when only checking atomic populations (thus, for 90° with regard to **3E**, the total electron population of O1 decreases, whereas that of O3 increases). Thus, this analysis reveals the effects of the π resonance, normally masked by ρ transferences from hydrogen atoms when regarding total atomic populations.

We also want to point out that internal rotation around C2−O3 shows that:

dx.doi.org/10.1021/ct400630f | J. Chem. Theory Comput. 2013, 9, 4816−4824

•Either in rigid or in relaxed scan, the O3−H4 moiety does not behave as an independent fragment with almost constant electron population (Supporting Information).

•From 50° to 130°, both O3 lone pairs are reflected by independent monosynaptic ELF basins that seem to interchange electron population. Both $N(V_{O3}^{1})$ and $N(V_{O3}^{2})$ display striking changes in that interval (Supporting Information).

4. CONCLUSIONS

The combination of both ELF and QTAIM basins gives rise to a new partitioning scheme which endows chemical significance to fragments defined within Bader's atomic basins. This work shows an interesting result, which is in line with chemical expectations: core and monosynaptic ELF basins are basically defined inside a single atomic basin. Moreover, ELF disynaptic basins can be divided into two sub-basins, belonging to each atom of the bond. Thus, one QTAIM atomic basin can be split into a core region, contributions to the bonds it is involved in, and lone pairs (if any). In the same vein, atomic contributions can be obtained for chemical bonds, defined through disynaptic ELF basins.

This new population analysis allows one to understand the conformational preferences of diverse anomeric compounds without invoking hyperconjugative effects. Thus, the ρ-restructure from the completely antiperiplanar arrangement to the most stable conformer basically involves (i) a ρ-reorganization within the oxygen atom (mainly an interchange between its lone pairs) and (ii) a ρ-transference from one H to the C−X region of the C basin.

Moreover, variation in electronic populations due to π resonance delocalizations, normally hidden when dealing only with QTAIM atomic populations, can be observed with this new ELF∩QTAIM scheme. In this fashion, some incompatibilities between QTAIM atomic populations and resonance model expectations could be explained.

■ ASSOCIATED CONTENT

Supporting Information

Tables S1−S8 report ELF contributions to the electron population of every QTAIM basin for the conformers here studied. Figure S1 shows a scheme of the ELF∩QTAIM superposition in the Z conformer of formic acid. Figures S2−S17 show the evolution of electronic populations of ELF∩QTAIM sub-basins along rigid and relaxed rotations for conformers here studied. This information in available free of charge via the Internet at http://pubs.acs.org/.

■ AUTHOR INFORMATION

Corresponding Authors

*E-mail: davidferro@uvigo.es.
*E-mail: mosquera@uvigo.es.

Notes

The authors declare no competing financial interest.

■ ACKNOWLEDGMENTS

The authors thank the Spanish Ministry of Economy for project CTQ2010-21500. D.F-C. also thanks the Spanish Ministry of Education for an FPU fellowship.

■ REFERENCES

(1) Bader, R. F. W. *Atoms in Molecules: A Quantum Theory*; Clarendon Press: Oxford, U. K., 1995.
(2) Bader, R. F. W. *Chem. Rev.* **1991**, *91*, 893−928.
(3) Becke, A. D.; Edgecombe, K. E. *J. Chem. Phys.* **1990**, *92*, 5397−5403.
(4) Savin, A.; Nesper, R.; Wengert, S.; Fässler, T. F. *Angew. Chem., Int. Ed. Engl.* **1997**, *36*, 1808−1832.
(5) Silvi, B.; Savin, A. *Nature* **1994**, *371*, 683−686.
(6) Chesnut, D. B. *J. Chem. Phys. A* **2000**, *104*, 11644−11650.
(7) Bader, R. F. W. *Pure Appl. Chem.* **1988**, *60*, 145−155.
(8) Juaristi, E.; Cuevas, G. *The Anomeric Effect*; CRC Press: Boca Raton, FL, 1995.
(9) Thatcher, G. R. J. *The Anomeric Effect and Associated Stereoelectronic Effects*; American Chemical Society: Washington, DC, 1993.
(10) Kirby, A. J. *The Anomeric Effect and Related Stereoelectronic Effects at Oxygen*; Springer-Verlag: Berlin, 1983.
(11) Edward, J. T. *Chem. Ind. (London)* **1955**, *36*, 1102−1104.
(12) Alabugin, I. V.; Gilmore, K. M.; Peterson, P. W. *Comput. Mol. Sci.* **2011**, *1*, 109−141.
(13) Cooper, D. *Valence Bond Theory*; Elsevier Science: Amsterdam, 2002; Vol. *10*.
(14) Heitler, W.; London, F. *Z. Phys.* **1927**, *44*, 455.
(15) Hurley, A. C.; Lennard-Jones, J. E.; Pople, J. A. *Proc. R. Soc. London* **1953**, *A220*, 446.
(16) Mo, Y. *Nat. Chem.* **2010**, *2*, 666−671.
(17) Ferro-Costas, D.; Otero, N.; Graña, A. M.; Mosquera, R. A. *J. Comput. Chem.* **2012**, *33*, 2533−2543.
(18) Blanco, M. A.; Pendás, A. M.; Francisco, E. *J. Chem. Theory Comput.* **2005**, *1*, 1096−1109.
(19) Ferro-Costas, D.; Vila, A.; Mosquera, R. A. *J. Phys. Chem. A* **2013**, *117*, 1641−1650.
(20) Vila, A.; Mosquera, R. A. *J. Comput. Chem.* **2007**, *28*, 1516−1530.
(21) The Electron Localization Function normally used is only defined for monodeterminantal systems. However, there are different generalizations which deal with multideterminantal wave functions.
(22) For the sake of simplicity, we only consider molecular systems with a maximum synaptic order equal to two in this expression.
(23) Tang, W.; Sanville, E.; Henkelman, G. *J. Phys.: Condens. Matter* **2009**, *21* (084204), 7.
(24) Lu, T.; Chen, F. *J. Comput. Chem.* **2012**, *33*, 580−592.
(25) The g-scan of methanediol is only performed in the 0° to 180° range, because of the high relative energy of the 2gg′ conformer[20] (the one with Cs symmetry).
(26) Frisch, M. J. et al. *Gaussian 09*, revision A.02.; Gaussian Inc.: Wallingford, CT, 2009.
(27) Bickelhaupt, F. M.; Baerends, E. J. *Angew. Chem., Int. Ed.* **2003**, *42*, 4183−4188.